ACS OMEGA

http://pubs.acs.org/journal/acsodf

Article

Naphthoquinoneoxime-Sensitized Titanium Dioxide Photoanodes: Photoelectrochemical Properties

Niyamat I. Beedri, Vivek B. Mokashi, Sharad A. Mahadik, Habib M. Pathan,* and Sunita Salunke-Gawali*

Cite This: *ACS Omega* 2022, 7, 41519−41530

Read Online

ACCESS | Metrics & More | Article Recommendations | Supporting Information

ABSTRACT: Naphthoquinoneoxime derivatives, viz., LwOx, 3-hydroxy-4-(hydroxyimino)naphthalen-1 (4*H*)-one; PthOx, 3-hydroxy-4-(hydroxyimino)-2-methylnaphthalen-1(4*H*)-one; and Cl_LwOx, 2-chloro-3-hydroxy-4-(hydroxyimino)naphthalen-1(4*H*)-one, are used in fabrication of dye-sensitized solar cells (DSSCs). The photophysical and electrochemical properties of the sensitizers were studied. The HOMO−LUMO energy gaps of the sensitizers (LwOx, PthOx, and Cl_LwOx) calculated by using the intersection of UV−visible and fluorescence spectra are 2.85, 2.71, and 2.87 eV, respectively. The energy band alignment energy level of the sensitizer, that is, the lowest unoccupied molecular orbital (LUMO) and highest occupied molecular orbital (HOMO), should match with the energy level of the TiO_2 conduction band and the redox potential of iodine/triiodide electrolyte to allow smooth electron transfer. The electrochemical characterization of sensitizers was done to find the LUMO and HOMO level of the sensitizer. It shows that the LUMO level of (LwOx, PthOx, and Cl_LwOx) is above the conduction band position of TiO_2. Electrochemical impedance spectroscopy was used to study the charge transport resistance and electron lifetime of DSSCs. The charge transport resistance at the TiO_2|electrolyte|counter electrode interface was reduced in the Cl_LwOx device; thus, the electron lifetime of Cl_LwOx was enhanced compared to LwOx and PthOx sensitizers. The fabricated device was characterized using photocurrent density−voltage (J−V) measurement. It is observed that there was an enhancement in the overall power conversion efficiency (η) of the DSSCs fabricated by using Cl_LwOx sensitizers as compared to LwOx and PthOx sensitizer-loaded photoanodes. Enhancement in power conversion efficiency, that is, photovoltage and photocurrent, is achieved due to the chlorine substituent. Thus, the chlorine substituent naphthoquinoneoxime pushes the electron density, enhancing the pushing nature and facilitating the lone pair present in the N−OH moiety to attach to TiO_2 more strongly.

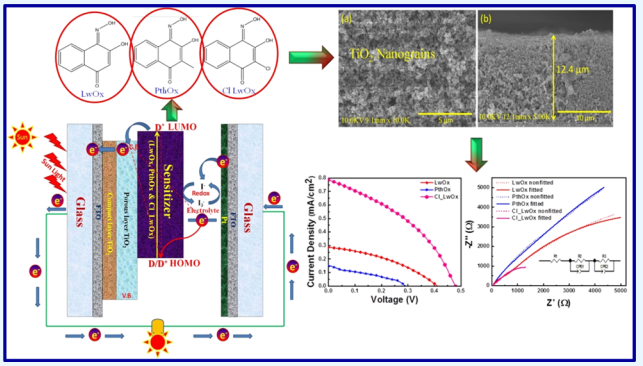

1. INTRODUCTION

Energy supply is the primary and momentous need for the development of human civilization. The world population is rapidly growing. Every individual needs the energy to fulfill their basic necessity. It is an essential requirement for an adequate standard of living. Energy crisis-related topics are the thrust areas of today's research. In the 21st century, a big challenge for humans is overcoming the energy crisis. Energy conversion is the process of capturing minute amounts of energy from energy sources, that is, the sun, and converting them into electricity for later use. An alternative for future large-scale energy production is photovoltaics.[1−3] Electricity generation from solar cells has emerged as one of the most promising and rapidly growing areas for power generation. There has always been a quest to find efficient and stable solar cell technology at a competitive cost.[4−6] Recently, a new kind of solar cell has emerged, which has shown great potential and promises to be more cost-effective and efficient than any other solar cell technology known thus far. These solar cells are called dye-sensitized solar cells (DSSCs).[7,8]

The production of cost-effective devices that can absorb sunlight and convert it into electricity is a crucial step in aiming at a sustainable society. Electricity production is needed for a revolutionary platform introducing clean and green energy modes such as DSSCs. The latest technologies are employed to make earth-abundant materials available on a large scale to fabricate wearable solar cells so that light harvesting can be maximized.[9−13] Compared to first-generation silicon solar cells and second-generation thin-film solar cell technology, mesoscopic DSSCs have less power conversion efficiency under

Received: August 19, 2022
Accepted: October 21, 2022
Published: November 3, 2022

ACS Publications

© 2022 The Authors. Published by American Chemical Society

Table 1. Comparison of Photovoltaic Performance of Several Quinone-Based Sensitizers with Different Photoanodes and Input Powers along with LwOx, PthOx, and Cl_LwOx Sensitizers

sensitizer	photoanode	P_{in} (mW/cm^2)	V_{oc} (V)	J_{sc} (mA/cm^2)	FF	η (%)	references
LwOx	TiO_2	100	0.41	0.28	37	0.04	present study
PthOx	TiO_2	100	0.28	0.15	32	0.01	present study
Cl_LwOx	TiO_2	100	0.47	0.78	38	0.14	present study
2-hydroxy-3-[phenyl(phenylamino)methyl] naphthalene-1,4-dione (4a)	TiO_2	100	0.29	0.035	50		33
HA3	ZnO	100	0.29	1.21	35	0.12	34
HA4	ZnO	100	0.32	0.71	38	0.09	34
BrA3	ZnO	100	0.33	1.01	39	0.13	34
BrA4	ZnO	100	0.31	1.66	38	0.20	34
4-OMe	TiO_2	100	0.36	0.053	57	0.01	35
4-Me	TiO_2	100	0.37	0.045	56	0.009	35
4-Br	TiO_2	100	0.34	0.034	58	0.007	35
4-Cl	TiO_2	100	0.31	0.026	54	0.004	35
2,4-diCl	TiO_2	100	0.26	0.022	46	0.003	35
4-(3-chloro-1, 4-dioxo-1, 4-dihydronaphthalen-2-ylamino)benzoic acid	ZnO	100	0.392	3.196	60	0.75	36
lawsone	ZnO	100	0.52	1.80	62	0.56	37
BPO_Cl	TiO_2	80	0.56	0.430			38
BPO	TiO_2	80	0.53	0.440			38
BPT	TiO_2	80	0.49	0.240			38
6-methyl-5*H*-benzo[α]henothiazine-5-one	ZrO_2	15	0.42	3.01	20	1.64	39
AMT	ZnO	100	0.21	0.17	60	0.02	40
AET	ZnO	100	0.22	0.22	59	0.03	40
AMT	TiO_2	100	0.41	1.73	33	0.23	40
AET	TiO_2	100	0.42	1.73	44	0.32	40

standard 1-sun conditions. Still, DSSCs show better power conversion efficiency under ambient or diffused light conditions.[14−16] The best 13% certified efficiency was achieved for laboratory-scale DSSCs. The research is appealing due to its low cost, simple fabrication process, transparency, application on flexible substrates, and high photon conversion efficiency.[17−22]

The efficiency of DSSCs is dependent primarily upon the sensitizer and the role of other components such as the photoanode material, electrolyte, and counter electrode, which are also essential in device fabrication. Usually, a ruthenium(II)-based light-absorbing sensitizer has been used in DSSCs; other than ruthenium(II)-based sensitizers, different metal complex-based sensitizers, natural dyes, and synthetic organic metal-free sensitizers[23−26] have also been used.

Synthetic organic metal-free dyes as sensitizers have attracted significant research interest due to their high molar extinction coefficients, tunable electronic structures, and light-harvesting ability.[27−29] Metal-free organic sensitizers are a viable alternative to metal-based sensitizers because of several advantages such as easy preparation, low cost, eco-friendly biodegradability, and wide availability. π-Conjugated sensitizers also play an important role in developing DSSCs due to their high polarizability, tunable spectroscopy, and electrochemical properties.[30] Depending on the number of ring structures, quinones are classified as benzoquinones, naphthoquinones, and anthraquinones. Naphthoquinone is the most common group of quinones found in nature. The commonly occurring isomers, 1,4-naphthoquinones, are the most stable.[31,32] Few reports are available on bare 1,4-naphthoquinone and the derivative of 1,4-naphthoquinone as a sensitizer in DSSCs. Chenab et al.[33] have used a 2-hydroxy-3-[phenyl(phenylamino)methyl]naphthalene-1,4-dione (4a) sensitizer in DSSC applications and observed acceptable photovoltaic performance. Mahadik et al.[34] reported that amino-naphthoquinone dye as a photosensitizer with ZnO photoanode enhances photovoltaic parameters due to decreased charge transport resistance.

Khanmohammadi et al.[35] did a comparative study to understand the effect of electron-withdrawing and electron-donating substitution on naphthoquinone dye with different substitutions on moiety parts that affect photovoltaic efficiency. Shinde et al.[36] studied the 4-(3-chloro-1,4-dioxo1,4-dihydro-naphthalen-2-ylamino) benzoic acid sensitizer using a simple chemical reaction. The sensitizer was examined computationally using density-functional theory (DFT) and time-dependent DFT (TD-DFT), and the photoelectrochemical properties of DSSCs were studied using ZnO as a photoanode. Khadtare et al.[37] reported lawsone (2-hydroxynaphthalene-1,4-dione)-sensitized ZnO photoanodes and tested DSSCs in addition to this spectral feature of lawsone explored using TD-DFT. Sahoo et al.[38] reported the application of a benzo[α]phenoxazine moiety as a sensitizer demonstrated through a DSSC device. Bhand et al.[39] studied the synthesis of benzo[α] phenothiazine as a sensitizer in ZrO_2 photoanode-based DSSCs. Mahadik et al.[40] investigated thionaphthoquinone dye as a sensitizer compared with ZnO nanograins and TiO_2 nanorod-based devices. Table 1 shows the comparison of the photovoltaic performance of different quinone-based sensitizers with different photoanodes and input powers along with LwOx, PthOx, and Cl_LwOx sensitizers. According to the literature, not a single attempt has been made for LwOx, PthOx, and Cl_LwOx sensitizers for TiO_2-based photoanodes toward DSSC application.

In the present work, we have used novel three derivatives of naphthoquinoneoxime, viz., LwOx, 3-hydroxy-4-(hydroxyimino)naphthalen-1(4*H*)-one; PthOx, 3-hydroxy-4-(hydroxyimino)-2-methylnaphthalen-1(4*H*)-one; and

https://doi.org/10.1021/acsomega.2c05334
ACS Omega 2022, 7, 41519−41530

Cl_LwOx, 2-chloro-3-hydroxy-4-(hydroxyimino)naphthalen-1(4*H*)-one. The molecular structures of sensitizers (LwOx, PthOx, and Cl_LwOx) are shown in Figure 1. The sensitizer

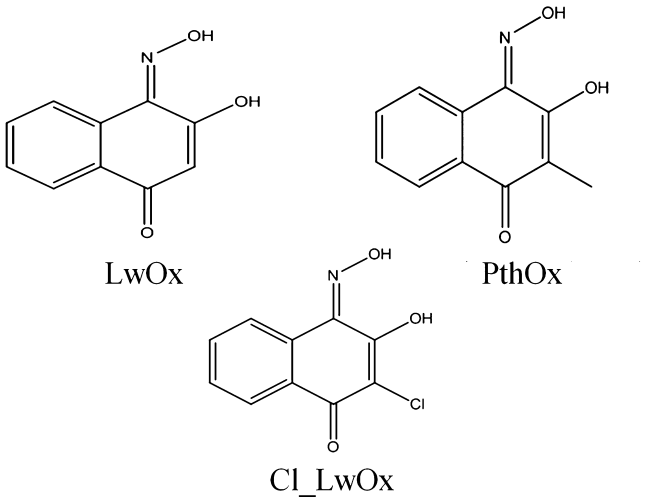

Figure 1. Molecular structures of sensitizers LwOx, PthOx, and Cl_LwOx.

contains specific suitable peripheral −OH (hydroxyl) anchoring groups for adsorption on the TiO_2 surface.[21,41−43] In the case of the Cl_LwOx-based sensitizer, the chlorine substituent naphthoquinoneoxime pushes the electron density, enhancing the pushing nature and facilitating the lone pair present in the N−OH moiety to attach with TiO_2 more strongly.

We used a doctor blade method to deposit the mesoporous TiO_2 photoanode; after that, the deposited photoanodes were characterized for their optical, morphological, and structural properties. DSSCs are fabricated by loading a sensitizer in ethanolic solutions of LwOx, PthOx, and Cl_LwOx on the photoanode. After sensitizer loading, the photovoltaic parameters of fabricated DSSCs measured in terms of the current density, open-circuit voltage, fill factor, efficiency, charge transport resistance, and effective electron lifetime of the fabricated (LwOx, PthOx, and Cl_LwOx) device are investigated in detail. The enhancement in power conversion efficiency is achieved for the Cl_LwOx-sensitized TiO_2 photoanode compared to LwOx and PthOx-sensitized DSSCs. The chlorine substituted naphthoquinoneoxime produces DSSCs having performance due to its bulky nature and availability of a lone pair on the chlorine moiety despite its position in the ring. The modified physicochemical properties due to chlorine attached to the naphthoquinoneoxime sensitizer and its impact on the DSSC are explained in brief in this report for the first time. The current investigation presents novel sensitizer (LwOx, PthOx, and Cl_LwOx) conjugation TiO_2-based DSSCs.

2. EXPERIMENTAL SECTION

2.1. Materials. For the preparation of TiO_2 paste, commercial TiO_2 P25 Degussa (Nanoshell LLC, USA) was used, followed by ethanol (Changshu, China), ethylcellulose (SDFCL), anhydrous α-terpineol (Kemphasol Ltd, India), and acetylacetone (HPCL, India) that were used as received. Fluorine-doped tin oxide (FTO) of sheet resistance 15−20 Ω/□ was purchased from Merck. A polyiodide solution was used as a liquid electrolyte consisting of lithium iodide (SRL, India), iodine (Fisher Scientific, USA), tertiary butyl pyridine (ACROS Organics, Belgium), and acetonitrile (SDFCL, India) used as received.

Scheme 1. Synthesis of Sensitizers: (a) LwOx; (b) PthOx; (c) Cl_LwOx

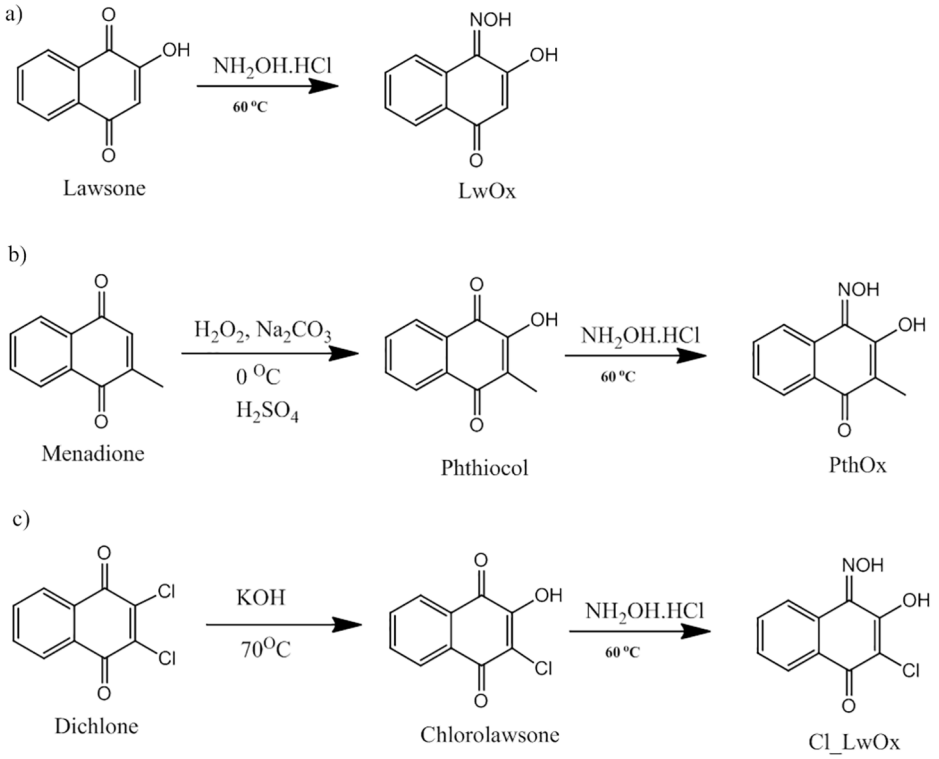

https://doi.org/10.1021/acsomega.2c05334
ACS Omega 2022, 7, 41519−41530

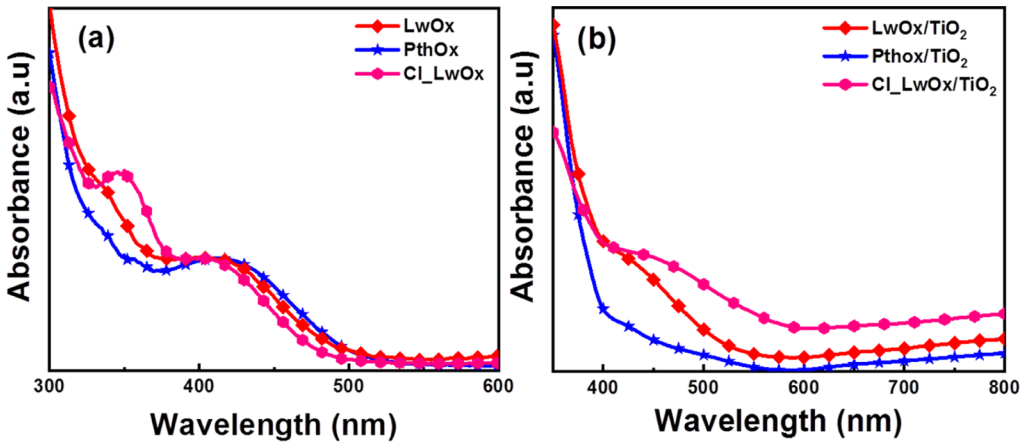

Figure 2. UV−visible spectra of (a) sensitizers LwOx, PthOx, and Cl_LwOx and (b) sensitizers LwOx-, PthOx-, and Cl_LwOx-loaded TiO_2 photoanodes.

2.2. General Procedure for the Synthesis of a Napthoquinoneoxime Derivative. LwOx, 3-hydroxy-4-(hydroxyimino) naphtalen-1(4*H*)-one; PthOx, 3-hydroxy-4-(hydroxyimino)-2-methylnaphtalen-1(4*H*)-one; and Cl_LwOx, 2-chloro-3-hydroxy-4-(hydroxyimino) naphthalen-1(4*H*)-one was synthesized by using Scheme 1a−c.

2.2.1. Synthesis of LwOx. LwOx was synthesized using Scheme 1a, treating lawsone(2-hydroxynaphthalene-1,4-dione) with hydroxylamine hydrochloride in a basic medium. The mixture was heated to 60 °C, cooled, and neutralized with hydrochloric acid (2 N), causing precipitation of LwOx.

2.2.2. Synthesis of PthOx. Phthiocol(2-hydroxy-3-methyl-naphthalene-1,4-dione) was synthesized using Scheme 1b initially using commercially available menadione, treated with hydrogen peroxide and epoxide as an intermediate. Ring opening of this epoxide intermediate was done with concentrated H_2SO_4. Addition of water afforded a yellow-color residue further recrystallized from methanol. PthOx was synthesized by treating the solution of phthiocol with the solution of hydroxylamine hydrochloride in a basic medium. The mixture was heated to 60 °C, cooled, and neutralized with hydrochloric acid (2 N), causing precipitation of PthOx.

2.2.3. Synthesis of Cl_LwOx. Scheme 1c was used for the synthesis of Cl_LwOx; initially, chlorolawsone(2-chloro-3-hydroxynaphthalene-1,4-dione) was synthesized from dichlone(2,3-dichloronaphthalene-1,4-dione). A methanolic solution of dichlone 2 N KOH was added with constant stirring. After heating the mixture for 1 h, a red precipitate was obtained. This precipitate was dissolved in warm water and neutralized with 2 N HCl, which yielded a yellow precipitate of chlorolawsone. The precipitate was filtered, washed with diethyl ether, and dried under a vacuum. Cl_LwOx was synthesized by treating the solution of chlorolawsone with the solution of hydroxylamine hydrochloride in a basic medium. The mixture was heated to 60 °C, cooled, and neutralized with hydrochloric acid (2 N), causing the precipitation of Cl_LwOx.

2.3. Fabrication of the TiO_2 Photoanode. Before the porous TiO_2 layer deposition, the compact TiO_2 layer was deposited using the chemical bath deposition technique as per a similar report.[44,45] A porous layer of TiO_2 was deposited using the doctor blade technique. First, a TiO_2 paste was made from commercially available TiO_2 powder (P25 Degussa) as the source material, using ethanol as the solvent, ethylcellulose as a binder, terpineol as the surfactant, and acetylacetone as a dispersant, similar to reported methods.[22,37,46] The prepared paste was deposited using the doctor blade method over a compact TiO_2 layer. After 15 min of drying, films were annealed for 1 h at 450 °C.

2.4. Instrumentation. The photoanode was characterized by X-ray diffraction (D/B max-2400, Rigaku, with Cu Kα, λ = 1.5406 Å) at 20−80°. The surface morphology and cross-section were observed using the field emission scanning electron microscopy (FE-SEM) technique (Carl Zeiss, Merlin Compact). The shape and size of TiO_2 nanoparticles were studied using transmission electron microscopy (TEM) Tecnai G^2 20 Twin, FEI. The optical absorption spectra of sensitizers were recorded using a SHIMADZU UV 1650 spectrophotometer from 200 to 600 nm, and emission spectra were measured using a JASCO spectrofluorometer FP-8300 between 410 and 550 nm. The excited-state lifetime of the sensitizer was measured using the time-correlated single-photon counting (TCSPC) method using a light-emitting diode (nano-LED) excited at 450 nm using a Fluorolog FL3 (FL-1057) instrument with a fast photomultiplier tube. The decay data was fitted with double-exponential decay. The FT-IR spectra were measured using a Bruker VERTEX by SHIMADZU FT 8400 spectrometer between 4000 and 400 cm^{-1} by the ATR technique. The electrochemical measurement was carried out using a CHI6054E electrochemical analyzer (CHI 660) at a scan rate of 0.1−0.5 V s^{-1} in ethanol against $Ag/AgNO_3$ (BAS) as a reference electrode. A commercial Pt disc electrode (CHI 102, surface area 0.025 cm^2) was used as the working electrode, and a platinum wire electrode (CHI 115) was used as the counter electrode at room temperature. Before starting each measurement, the analyte was deoxygenated by argon purging.

2.5. Fabrication of DSSCs. Annealed TiO_2 films were dipped for 72 h in 0.05 M LwOx, PthOx, and Cl_LwOx sensitizer solutions prepared in ethanol. The liquid polyiodide electrolyte was prepared similarly as reported in our previous work.[22] Then, the prepared polyiodide electrolyte was introduced between the sensitizer-loaded photoanode, coupled with a Pt counter electrode using binder clips. The assembled devices have been studied using the photocurrent density−voltage (J−V) characteristic curves obtained for an active cell area (0.25 cm^2) generated using a Keithley 2400 source meter and solar simulator (Enlitech model SS-F5-3A) with an

https://doi.org/10.1021/acsomega.2c05334
ACS Omega 2022, 7, 41519−41530

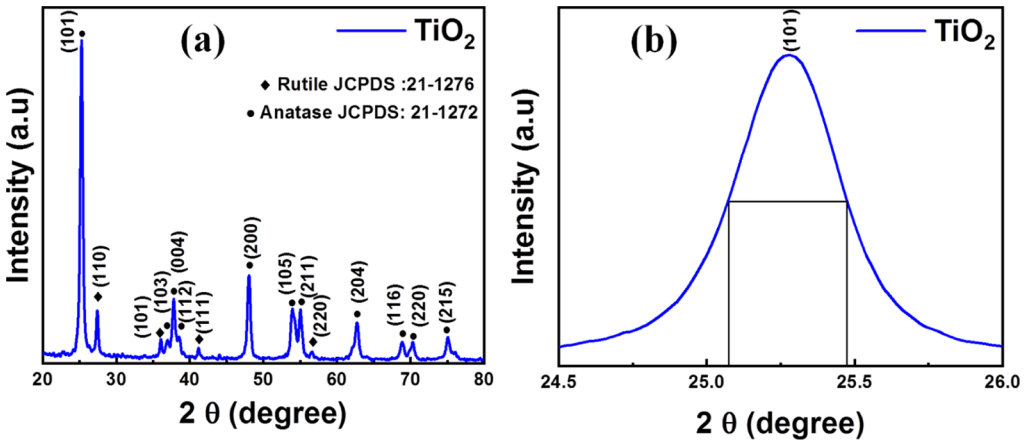

Figure 3. (a) XRD patterns of TiO_2. (b) Crystallite size calculation.

incident light intensity 100 mW cm^{-2}. The electrochemical impedance spectroscopy (EIS) measurements for DSSCs were carried out using a potentiostat/galvanostat (IVIUM: Vertex) to study the TiO_2/LwOx, PthOx, and Cl_LwOx/electrolyte interface in the frequency domain of 10^6 to 10^0 Hz) in the dark with applied voltage, which was open-circuit voltage.

3. RESULTS AND DISCUSSION

3.1. Optical Absorption Measurements. Figure 2a,b shows the optical absorption spectra of sensitizers and sensitizer-loaded TiO_2 photoanodes. Figure 2a shows the optical absorbance for ethanolic solutions of LwOx, PthOx, and Cl_LwOx sensitizers as a function of wavelength. Absorptions ranges were observed for LwOx between 386 and 510 nm, and PthOx absorption was seen from 350 to 500 nm; similarly, Cl_LwOx absorption was seen from 380 to 523 nm.

The maximum absorption wavelength (λ_{max}) for LwOx, PthOx, and Cl_LwOx sensitizers was ~407, 413, and 402 nm, respectively. The sensitizer-loaded TiO_2 photoanodes' UV−visible absorbance spectra are shown in Figure 2b, with the maximum absorption wavelength (λ_{max}) observed at 425, 422, and 420 nm, respectively. The red shift toward the longer wavelength in the visible region for all sensitizer-loaded TiO_2 photoanodes confirms the formation of complexation between the sensitizer and TiO_2, which shows the sufficient amount of the sensitizer adsorb on the TiO_2 surface.[47,48] The UV−visible absorbance spectra of all three sensitizers show the absorption in ultraviolet and visible-region bands assigned to $\pi \rightarrow \pi^*$ and $n \rightarrow \pi^*$ charge transfer, respectively.[49] The absorption data for bare TiO_2 were analyzed, and the TiO_2 band gap was 3.2 eV. Figure S1 shows the optical properties of TiO_2 photoanodes. The inset shows the plot of $(\alpha h\nu)^2$ versus energy ($h\nu$). The estimated band gap of TiO_2 agrees with the previously reported results.[50−53]

3.2. Structural Characterization. Figure 3a,b shows the X-ray diffraction (XRD) pattern and full-width half-maximum (fwhm) peak for crystallite size calculation of TiO_2. The experimental planes were (101), (110), (103), (200), (004), (112), (111), (200), (105), (211), (220), (204), (116), (220), and (215). The XRD pattern in Figure 3a was compared with standard data and matched with JCPDS card no. 21-1272 for anatase and JCPDS card no. 21-1276 for rutile. Planes (101) and (110) show the characteristic peaks of anatase and rutile,[54−56] respectively.

Figure 3b shows the fwhm of (101) peaks. The crystallite size of TiO_2 (101) peaks is calculated using Scherer's formula.[57,58]

$$D = \frac{0.9\,\lambda}{\beta \mathrm{Cos}\theta} \quad (1)$$

where β is the full width in radians at the half-maximum of diffraction peaks, λ is the wavelength of the X-rays (λ = 1.54 Å), and θ is Bragg's angle of the X-ray pattern at maximum intensity. The crystallite size is ~42 nm.

3.3. Morphological Analysis. The FE-SEM technique was used to study the surface morphology of the TiO_2 photoanode. Figure 4a shows the FE-SEM images of the

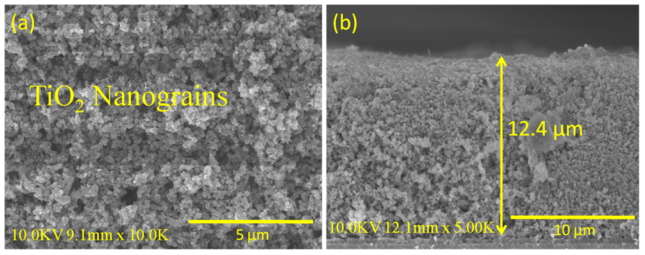

Figure 4. Surface morphology of (a) TiO_2 nanograins and (b) thickness of the TiO_2 photoanode.

TiO_2 layer, which shows a nanograin-like morphology. TiO_2 nanograins were deposited by the doctor blade method, and a highly dense, closely interconnected, and mesoporous morphology of TiO_2 has a significant role in better light harvesting since light harvesting depends upon the amount of sensitizer adsorbed on the photoanode surface.[59−63]Figure 4b shows a cross-sectional view of the TiO_2 photoanode showing a 12.4 μm thickness.

3.4. Transmission Electron Microscopy. TEM images were taken to study the photoanode material morphology and particle size. TiO_2 particle assembly showed a mesoporous character with excellent connectivity among the particles with an apparent cuboidal morphology,[64,65] as shown in Figure 5a. The TEM image shows that the TiO_2 particle has good connectivity and bond strength, which offers a large surface area for sensitizer adsorption, and interparticle connectivity facilitates electron diffusion through TiO_2. The average particle size range of TiO_2 nanoparticles is nearly 25 nm, as measured

https://doi.org/10.1021/acsomega.2c05334
ACS Omega 2022, 7, 41519−41530

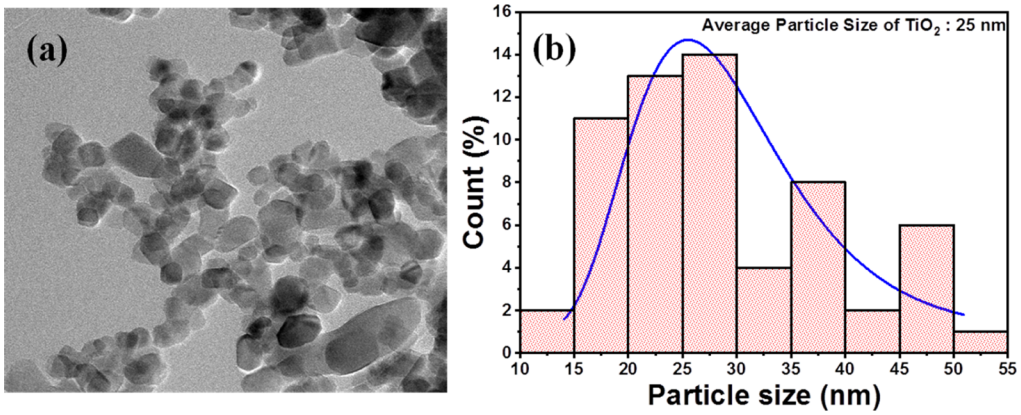

Figure 5. (a)TEM images of TiO_2 nanograins. (b) TiO_2 nanograin particle size distribution.

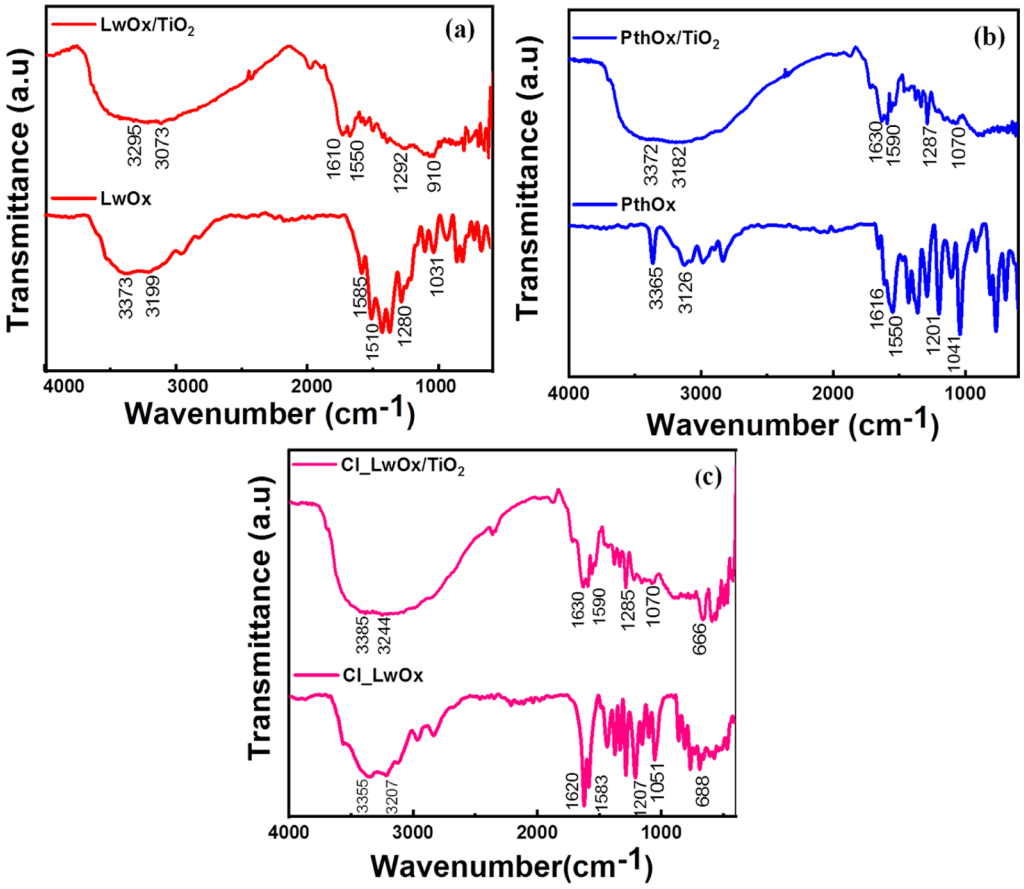

Figure 6. FT-IR spectra of the (a) sensitizer LwOx and LwOx-loaded TiO_2 photoanode, (b) sensitizer PthOx and PthOx-loaded TiO_2 photoanode, and (c) sensitizer Cl_LwOx and Cl_LwOx-loaded TiO_2 photoanode.

Table 2. FT-IR frequencies of LwOx, PthOx, and Cl_LwOx Sensitizers and Sensitizer-Loaded Photoanodes

	FT-IR frequency (cm^{-1})					
	LwOx		PthOx		Cl_LwOx	
functional group	sensitizer	sensitizer-loaded photoanode	sensitizer	sensitizer-loaded photoanode	sensitizers	sensitizer-loaded photoanode
ν_{OH}	3373	3295	3365	3372	3355	3385
	3199	3073	3126	3182	3207	3244
$\nu_{C=N}$	1602	1615	1616	1630	1620	1630
$\nu_{C=C}$	1510	1550	1550	1590	1583	1590
ν_{C-O}	1280	1292	1201	1287	1207	1285
ν_{N-O}	1031	910	1041	1070	1051	1070
ν_{C-Cl}					688	666

https://doi.org/10.1021/acsomega.2c05334
ACS Omega 2022, 7, 41519−41530

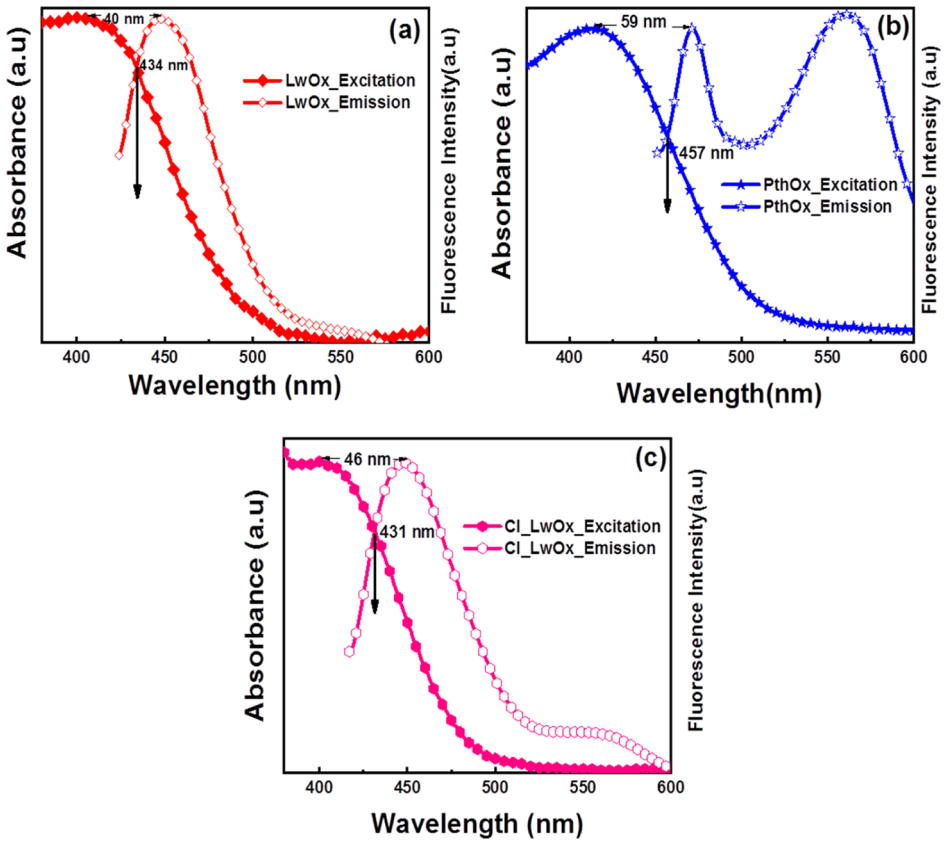

Figure 7. Combination of UV−visible (excitation) and fluorescence (emission) spectra of the (a) sensitizer LwOx, (b) sensitizer PthOx, and (c) sensitizer Cl_LwOx.

Table 3. Photophysical and Electrochemical Data of LwOx, PthOx, and Cl_LwOx Sensitizers

sensitizer	λ_{max} (nm)	λ_{PL} (nm)	Stokes shift (nm)	E_{0-0} (eV)	E_{HOMO} (eV)	E_{LOMO} (eV)	excited-state lifetime (ns)
LwOx	407	447	40	2.85	−6.50	−3.65	1.89
PthOx	413	472	59	2.71	−6.59	−3.88	1.74
Cl_LwOx	402	448	46	2.87	−6.56	−3.85	1.52

from the TEM image. The particle size distribution of TiO_2 was studied from the TEM image in Figure 5b.

3.5. FT-IR Spectroscopy Analysis. Figure 6a−c shows the FT-IR spectra of sensitizers and the sensitizer-loaded TiO_2 photoanode. The frequency bands of the LwOx, PthOx, and Cl_LwOx sensitizers were compared with those of the sensitizer-loaded TiO_2 photoanode, which shows a bonding interaction.[66,67] The selected frequency band of the bare sensitizer and sensitizer-loaded TiO_2 photoanode are summarized in Table 2.

LwOx, PthOx, and Cl_LwOx show a medium broad band at 3100−3600 cm^{-1} due to the free hydroxyl group (O−H) stretching frequency of oxime and phenolic hydroxyls.[68,69] The ν_{OH} band of the sensitizers LwOx(3373, 3199 cm^{-1}), PthOx (3365, 3126 cm^{-1}), and Cl_LwOx (3355, 3207 cm^{-1}) shifts to (3295, 3073 cm^{-1}), (3372, 3182 cm^{-1}), and (3385, 3244 cm^{-1}), respectively, in the sensitizer-loaded TiO_2 photoanode, as shown in Figure 6a−c.

In bare LwOx, PthOx, and Cl_LwOx sensitizers, the $\nu_{C=N}$ stretching frequency at ∼1602, 1616, and 1620 cm^{-1} is shifted to 1615, 1630, and 1630 cm^{-1}, respectively, in the sensitizer-loaded TiO_2 photoanode. After sensitizer loading, a noticeable shift of (13−25 cm^{-1}) was observed, confirming the added interaction between the sensitizer and TiO_2 photoanode. Sensitizers used in these studies have nitrogen and oxygen electron donor atoms.[70] LwOx, PthOx, and Cl_LwOx sensitizers have peaks at ∼1510, 1550, and 1583 cm^{-1}, respectively, due to the $\nu_{C=C}$ stretching frequency being shifted to (7−40 cm^{-1}) toward a higher wavenumber (bathochromic shift) as shown in Table 2.

The ν_{C-O} stretching frequencies for sensitizers LwOx, PthOx, and Cl_LwOx found at ∼1280, 1201, and 1207 cm^{-1} are shifted to higher wavenumbers at ∼ 1292, 1287, and 1285 cm^{-1}, respectively, in the sensitizer-loaded TiO_2 photoanode. The FT-IR bands at ∼1031, 1041, and 1051 cm^{-1} in the spectra of PthOx, LwOx, and Cl_LwOx are assigned to the (N−O) stretching frequency, which shifts to 19−29 cm^{-1} toward higher wavenumbers as shown in Table 2. In Cl_LwOx, the ν_{C-Cl} band frequency is found at ∼688 cm^{-1} and shifts to a lower wavenumber (∼666 cm^{-1}) by 22 cm^{-1}, as shown in Figure 6c.

3.6. Fluorescence Spectrum Analysis. Figure 7a−c shows the UV−visible (excitation) and fluorescence (emission) spectra of the sensitizers LwOx, PthOx, and Cl_LwOx. The fluorescence (emission) spectra of LwOx, PthOx, and Cl_LwOx sensitizers are measured, and the fluorescence emission maxima values are shown in Table 3.

https://doi.org/10.1021/acsomega.2c05334
ACS Omega 2022, 7, 41519−41530

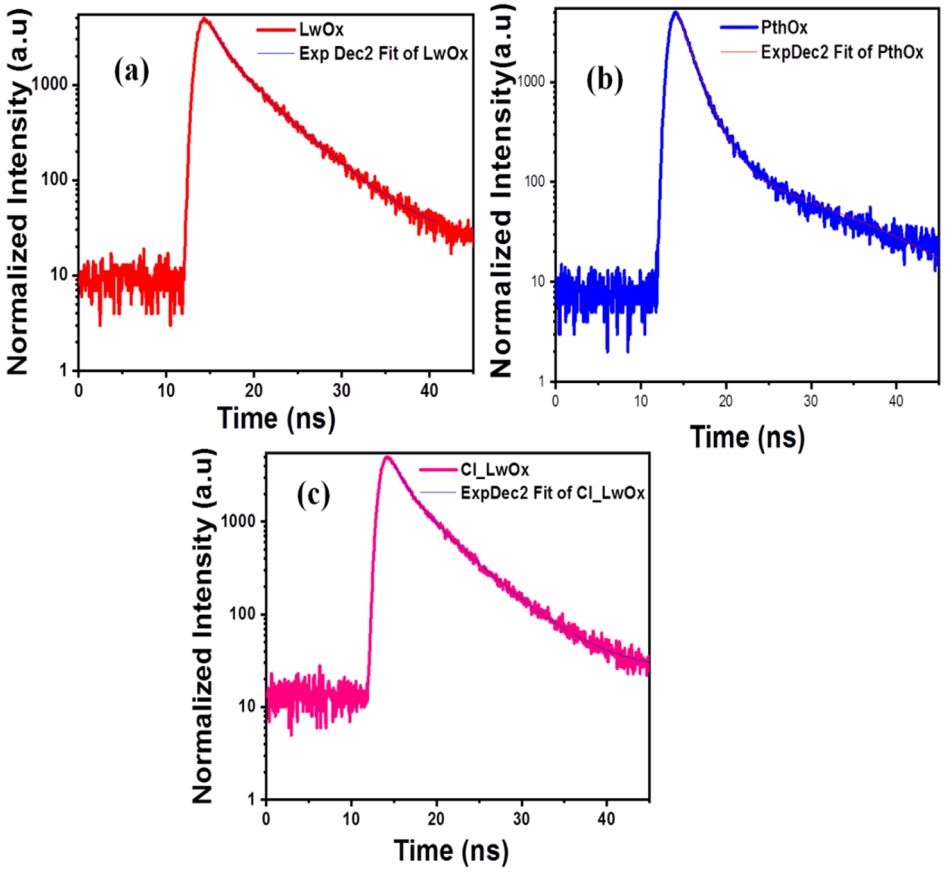

Figure 8. Excited-state lifetime data of the (a) sensitizer LwOx, (b) sensitizer PthOx, and (c) sensitizer Cl_LwOx.

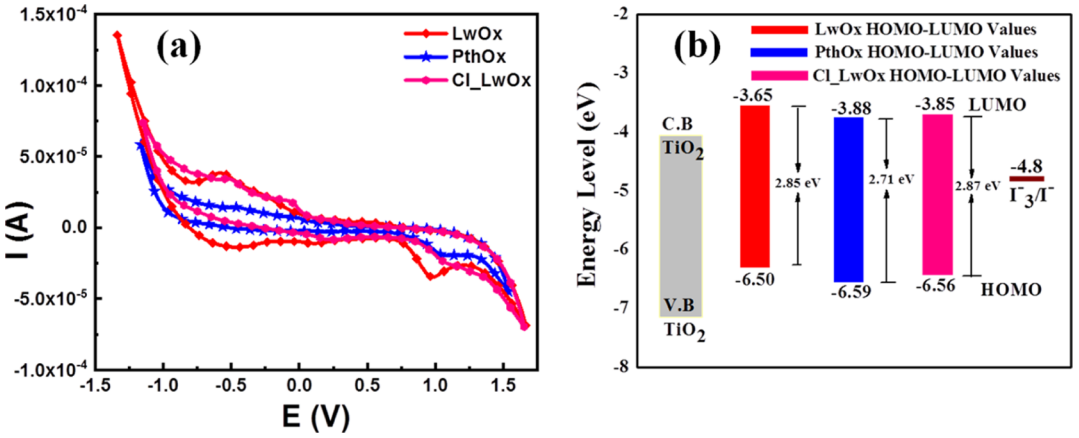

Figure 9. (a) Cyclic voltammograms of sensitizers LwOx, PhthOx, and Cl_LwO. (b) HOMO−LUMO comparison plot with the CB of TiO_2 and redox potential of I^-/I_3^-.

It shows fluorescence emission maxima at ∼447, 472, and 448 nm with a stock shift of 40, 59, and 46 nm for LwOx, PthOx, and Cl_LwOx sensitizers, respectively. The energy gap, that is, the HOMO−LUMO difference, was measured from the intersection of excitation and emission spectra of bare sensitizers.[71] The energy gap denoted by E_{0-0} is the difference between the excited and ground states. The E_{0-0} values of sensitizers LwOx, PthOx, and Cl_LwOx are 2.85, 2.71, and 2.87 eV, as shown in Table 3.

The time-dependent photoluminescence (PL) spectra of LwOx, PthOx, and Cl_LwOx sensitizers are measured and shown in Figure 8. The time-dependent PL spectrum was measured by TCSPC, which shows that the carrier lifetimes of sensitizers LwOx, PthOx, and Cl_LwOx are 1.89, 1.74, and 1.52 ns, respectively. The data were fitted with double-exponential decay. The carrier lifetime decay for Cl_LwOx is faster than that for PthOx and LwOx sensitizers. Excited-state lifetime data are summarized in Table 3.

3.7. Electrochemical Characterization. Figure 9a shows the electrochemical behavior of sensitizers LwOx, PthOx, and Cl_LwOx in ethanol solution. The electrochemical characterization of sensitizers was performed to find the lowest unoccupied molecular orbital (LUMO) and highest occupied molecular orbital (HOMO) level of the sensitizers LwOx,

https://doi.org/10.1021/acsomega.2c05334
ACS Omega 2022, 7, 41519−41530

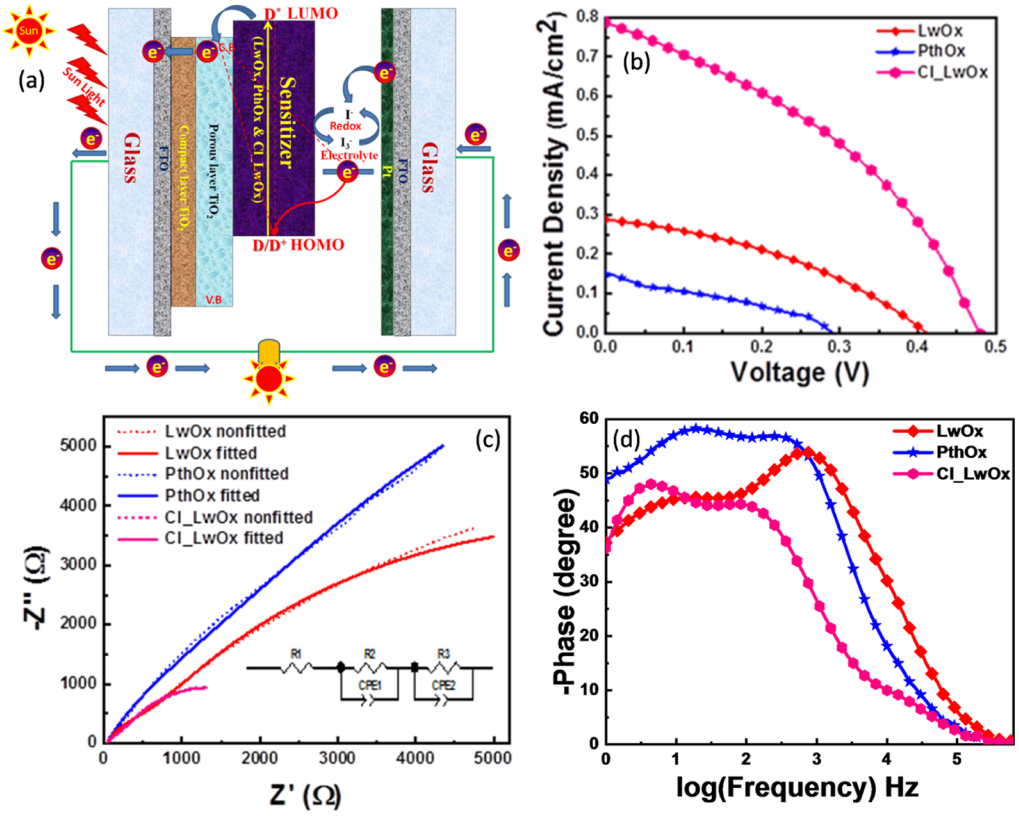

Figure 10. (a) Schematic of the process involved in DSSCs. (b) *J*–*V* characteristic. (c) Nyquist plot. (d) Bode plots of DSSCs based on LwOx-, PthOx-, and Cl_LwOx-sensitized TiO_2 photoanodes.

Table 4. Photovoltaic and Electrochemical Performance of TiO_2/LwOx, TiO_2/PthOx, and TiO_2/Cl_LwOx Photoanode Devices

photosensitizers	V_{oc} (V)	J_{sc}(mA/cm^2)	FF	R_1 (Ω)	R_2 (Ω)	τ_e (ms)	η (%)
LwOx	0.41	0.28	37	399	12187	10.04	0.04
PthOx	0.28	0.15	32	1912	21393	8.35	0.01
Cl_LwOx	0.47	0.78	38	461	1887	36.52	0.14

PthOx, and Cl_LwOx, respectively. Cyclic voltammetry experiments were performed using a three-electrode system at different scan rates of 0.1–0.5 V/s. The HOMO and LUMO energy levels of the sensitizers LwOx, PthOx, and Cl_LwOx are evaluated using the cyclic voltammetry technique, as shown in Figure 9a.

The HOMO–LUMO difference was calculated from Figure 7a–c and combined with the cyclic voltammetry Figure 9a data. Table 3 summarizes that the Cl_LwOx shows the highest HOMO–LUMO band difference of 2.87 eV among all three sensitizers, whereas the PthOx sensitizer shows the lowest 2.71 eV. The optoelectrical and electrochemical parameters are shown in Figure 9b and Table 3. It shows that the conduction band position of TiO_2 is below the LUMO level of LwOx, PthOx, and Cl_LwOx, and the redox potential of iodine/triiodide (−4.8 eV)[72] is above the HOMO level of the LwOx, PthOx, and Cl_LwOx sensitizers. The regeneration of dye in all the devices can be adequate with a driving force from 1.7 to 1.76 eV, which is enough for dye regeneration.

3.8. Characterization of DSSCs. *3.8.1. J–V and EIS Analysis.* The schematic diagram in Figure 10a shows a charge transfer process in DSSCs for FTO/TiO_2/(LwOx, PthOx, and Cl_LwOx) sensitizers/electrolyte/Pt. The sensitizer absorbs the photon, and the LwOx, PthOx, and Cl_LwOx molecules at the HOMO level get excited to the LUMO. The position of the LUMO level for LwOx, PthOx, and Cl_LwOx lies above the conduction band position of TiO_2, and the redox potential of iodine/triiodide (I^-/I_3^-) is above the HOMO level of LwOx, PthOx, and Cl_LwOx so that electron transfer can take place easily. A TiO_2 compact layer is used to avoid the direct access of electrolytes to the FTO surface. There is a probability that some other reaction can occur, such as recombining an injected electron to recombine with an oxidized sensitizer or electrolyte, resulting in the loss of the electron and a decrease in the fabricated device performance.[73−76]

Figure 10b shows the *J*–*V* characteristics of DSSCs fabricated using TiO_2 photoanodes sensitized with LwOx, PthOx, and Cl_LwOx sensitizers. The obtained result indicates that the Cl_LwOx sensitizer performs better than PthOx and LwOx sensitizer-based DSSCs. Cl_LwOx sensitization offers a higher value of J_{sc} due to an increase in the visible absorption range toward a higher wavelength after loading the Cl_LwOx sensitizer. The fabricated device parameters are summarized in Table 4.

EIS is used to study the charge transport at the counter electrode–electrolyte interface R_1 and charge transport resistance R_2 related to the charge transport resistance at the interface TiO_2|electrolyte|counter electrode. EIS measurement

https://doi.org/10.1021/acsomega.2c05334
ACS Omega 2022, 7, 41519−41530

was performed under open-circuit voltage and dark illumination conditions. The Nyquist plots of LwOx-, PthOx-, and Cl_LwOx-sensitized TiO_2 photoanode-based DSSCs are shown in Figure 10c. The Nyquist plot was fitted using Z View software to determine the electrochemical parameters of all three devices. R_2 is equivalent to circuit-fitted parameters. The value of R_2 is summarized in Table 4. The result shows that charge transport resistance at the interface TiO_2|sensitizer|electrolyte is more significant for PthOx than LwOx and Cl_LwOx sensitizer-based devices. Due to the lower charge transport resistance of the Cl_LwOx-based device, the electron lifetime increases, resulting in increased device efficiency.

The Bode phase plot is shown in Figure 10d. The effective electron lifetime (τ_{eff}) of fabricated devices can be calculated using equation[77,78]

$$\tau_{eff} = \frac{1}{2\pi f_{max}} \quad (2)$$

The good electron lifetime (τ_{eff}) for the DSSCs fabricated with LwOx, PthOx, and Cl_LwOx sensitizer is 10.04, 8.35, and 36.52 ms, respectively. The significant increase in the τ_{eff} value shows the efficient decrease of charge transport resistance between TiO_2|electrolyte|counter electrode interfaces in Cl_LwOx-sensitized TiO_2 photoanode-based DSSCs. The results show that chlorine substitution on the lawsoneoxime skeleton reduces charge transport resistance.

4. CONCLUSIONS

LwOx, PthOx, and Cl_LwOx were sensitized with TiO_2 photoanode-based DSSCs. The UV−visible absorbance spectra confirm that the sensitizers (LwOx, PthOx, and Cl_LwOx) absorb light due to $\pi \rightarrow \pi^*$ transition in the ultraviolet region and n $\rightarrow \pi^*$ transition in the visible region. The electrochemical characterization of the sensitizer was carried out to confirm that the CB level of TiO_2 is below the LUMO level of the sensitizer (LwOx, PthOx, and Cl_LwOx) so that electron injection can take place easily. The TiO_2 photoanode was prepared by the doctor blade technique. The FE-SEM image shows a porous surface morphology. The sensitizer was successfully adsorbed on a porous TiO_2 surface by the dipping method. The obtained results indicate that naphthoquinoneoxime derivatives can be potentially used as a sensitizer in TiO_2 photoanode-based DSSCs production due to their optoelectrical, structural, and functional nature. It is observed that the introduction of a chlorine substitute in naphthoquinoneoxime-based sensitizers reduces the charge transport resistance in naphthoquinoneoxime-based DSSCs, which results in the improvement of photovoltaic performance significantly. The study reveals that the naphthoquinoneoxime derivative compound can synthesize novel metal complex compounds with other donor−acceptor groups to enhance device efficiency.

ASSOCIATED CONTENT

Supporting Information

The Supporting Information is available free of charge at https://pubs.acs.org/doi/10.1021/acsomega.2c05334.

Optical properties of TiO_2 photoanodes, with the inset showing the plot of $(\alpha h\nu)^2$ versus energy $(h\nu)$ (PDF)

AUTHOR INFORMATION

Corresponding Authors

Habib M. Pathan − *Advanced Physics Laboratory, Department of Physics, Savitribai Phule Pune University, Pune 411 007, India*; Email: pathan@physics.unipune.ac.in

Sunita Salunke-Gawali − *Department of Chemistry, Savitribai Phule Pune University, Pune 411 007, India*; orcid.org/0000-0002-4460-3992; Email: sunita.salunke@unipune.ac.in

Authors

Niyamat I. Beedri − *Department of Chemistry, Savitribai Phule Pune University, Pune 411 007, India*; orcid.org/0000-0002-8357-0257

Vivek B. Mokashi − *Department of Chemistry, Savitribai Phule Pune University, Pune 411 007, India*

Sharad A. Mahadik − *Department of Chemistry, Savitribai Phule Pune University, Pune 411 007, India*

Complete contact information is available at: https://pubs.acs.org/10.1021/acsomega.2c05334

Notes

The authors declare no competing financial interest.

ACKNOWLEDGMENTS

N.I.B. is thankful for the Savitribai Phule Pune University Postdoctoral Fellowship (SPPU-PDF) program (grant no. SPPU-PDF/ST/PH/2021/0003).

REFERENCES

(1) Devadiga, D.; Selvakumar, M.; Shetty, P.; Santosh, M. S. The integration of flexible dye-sensitized solar cells and storage devices towards wearable self-charging power systems: a review. *Renew. Sustain. Energy Rev.* **2022**, *159*, 112252.

(2) Alizadeh, A.; Roudgar-Amoli, M.; Bonyad-Shekalgourabi, S.-M.; Shariatinia, Z.; Mahmoudi, M.; Saadat, F. Dye sensitized solar cells go beyond using perovskite and spinel inorganic materials: A review. *Renew. Sustain. Energy Rev* **2022**, *157*, 112047.

(3) Niedzwiedzki, D. M. Photophysical Properties of N719 and Z907 Dyes, Benchmark Sensitizers for Dye-Sensitized Solar Cells, at Room and Low Temperature. *Phys. Chem. Chem. Phys.* **2021**, *23*, 6182−6189.

(4) Deng, K.; Cole, J. M.; Rawle, J. L.; Nicklin, C.; Chen, H.; Yanguas-Gil, A.; Elam, J. W.; Stenning, G. B. G. Dye Nanoaggregate Structures in MK-2, N3, and N749 Dye···TiO_2 Interfaces That Represent Dye-Sensitized Solar Cell Working Electrodes. *ACS Appl. Energy Mater.* **2020**, *3*, 900−914.

(5) Borbón, S.; Lugo, S.; Pourjafari, D.; Aguilar, N. P.; Oskam, G.; López, I. Open-Circuit Voltage (V_{OC}) Enhancement in TiO_2-Based DSSCs: Incorporation of ZnO Nanoflowers and Au Nanoparticles. *ACS Omega* **2020**, *5*, 10977−10986.

(6) González-Verjan, V. A.; Trujillo-Navarrete, B.; Félix-Navarro, R. M.; Díaz de León, J. N.; Romo-Herrera, J. M.; Calva-Yáñez, J. C.; Hernández-Lizalde, J. M.; Reynoso-Soto, E. A. Effect of TiO_2 particle and pore size on DSSC efficiency. *Mater Renew Sustain Energy* **2020**, *9*, 13.

(7) Abrol, S. A.; Bhargava, C.; Sharma, P. K. Fabrication of DSSC Using Doctor Blades Method Incorporating Polymer Electrolytes. *Mater. Res. Express* **2021**, *8*, 045010.

(8) Devadiga, D.; Selvakumar, M.; Devadiga, D.; Paramasivam, S.; Ahipa, T. N.; Shetty, P.; Kumar, S. S. Organic sensitizer with azine π-conjugated architecture as co-sensitizer and polymer-based electrolyte for efficient dye-sensitized solar cell. *Surface. Interfac* **2022**, *33*, 102236.

(9) Lunt, R. R.; Osedach, T. P.; Brown, P. R.; Rowehl, J. A.; Bulović, V. Practical Roadmap, and Limits to Nanostructured Photovoltaics. *Adv. Mater.* **2011**, *23*, 5712−5727.
(10) Chen, G.; Seo, J.; Yang, C.; Prasad, P. N. Nanochemistry and Nanomaterials for Photovoltaics. *Chem. Soc. Rev.* **2013**, *42*, 8304−8338.
(11) Fakharuddin, A.; Jose, R.; Brown, T. M.; Fabregat-Santiago, F.; Bisquert, J. A Perspective on the Production of Dye-Sensitized Solar Modules. *Energy Environ. Sci.* **2014**, *7*, 3952−3981.
(12) Husain, A. A. F.; Hasan, W. Z. W.; Shafie, S.; Hamidon, M. N.; Pandey, S. S. A Review of Transparent Solar Photovoltaic Technologies. *Renew. Sustain. Energy Rev.* **2018**, *94*, 779−791.
(13) Parida, B.; Iniyan, S.; Goic, R. A Review of Solar Photovoltaic Technologies. *Renew. Sustain. Energy Rev.* **2011**, *15*, 1625−1636.
(14) Freitag, M.; Teuscher, J.; Saygili, Y.; Zhang, X.; Giordano, F.; Liska, P.; Hua, J.; Zakeeruddin, S. M.; Moser, J.-E.; Grätzel, M.; Hagfeldt, A. Dye-Sensitized Solar Cells for Efficient Power Generation under Ambient Lighting. *Nat. Photonics* **2017**, *11*, 372−378.
(15) Jagtap, C. V.; Kadam, V. S.; Jadkar, S. R.; Pathan, H. M. Performance of N3 Sensitized Titania Solar Cell under Artificial Light Ambience. *ES Energy Environ.* **2019**, *3*, 60−67.
(16) O'Regan, B.; Grätzel, M. A Low-Cost, High-Efficiency Solar Cell Based on Dye-Sensitized Colloidal TiO2 Films. *Nature* **1991**, *353*, 737−740.
(17) Ludin, N. A.; Al-Alwani Mahmoud, A. M.; Bakar Mohamad, A.; Kadhum, A.. A. H.; Sopian, K.; Abdul Karim, N. S. Review on the Development of Natural Dye Photosensitizer for Dye-Sensitized Solar Cells. *Renew. Sustain. Energy Rev.* **2014**, *31*, 386−396.
(18) Yao, Z.; Zhang, M.; Wu, H.; Yang, L.; Li, R.; Wang, P. Donor/Acceptor Indenoperylene Dye for Highly Efficient Organic Dye-Sensitized Solar Cells. *J. Am. Chem. Soc.* **2015**, *137*, 3799−3802.
(19) Zhang, D.; et al. A Molecular Photosensitizer Achieves a V_{oc} Of 1.24 V Enabling Highly Efficient and Stabledye-Sensitized Solar Cells with Copper(II/I)-Based electrolyte. *Nat. Commun.* **2021**, *12*, 1777.
(20) Zhang, M.; Wang, Y.; Xu, M.; Ma, W.; Li, R.; Wang, P. Design of High-Efficiency Organic Dyes for Titania Solar Cells Based on the Chromophoric Core of Cyclopentadithiophene-Benzothiadiazole. *Energy Environ. Sci.* **2013**, *6*, 2944.
(21) Hagfeldt, A.; Boschloo, G.; Sun, L.; Kloo, L.; Pettersson, H. Dye-Sensitized Solar Cells. *Chem. Rev.* **2010**, *110*, 6595−6663.
(22) Beedri, N. I.; Baviskar, P. K.; Bhalekar, V. P.; Jagtap, C. V.; Asiri, A. M.; Jadkar, S. R.; Pathan, H. M. N3-Sensitized TiO_2/Nb_2O_5: A Novel Bilayer Structure for Dye-Sensitized Solar-Cell Application. *Phys. Status Solidi A* **2018**, *215*, 1800236.
(23) Li, J.; Yang, X.; Yu, Z.; Gurzadyan, G. G.; Cheng, M.; Zhang, F.; Cong, J.; Wang, W.; Wang, H.; Li, X.; Kloo, L.; Wang, M.; Sun, L. Efficient Dye-Sensitized Solar Cells with [Copper(6,6′-Dimethyl-2,2′-Bipyridine) $_2$] $^{2+/1+}$ Redox Shuttle. *RSC Adv.* **2017**, *7*, 4611−4615.
(24) Kang, M. S.; Kang, S. H.; Kim, S. G.; Choi, I. T.; Ryu, J. H.; Ju, M. J.; Cho, D.; Lee, J. Y.; Kim, H. K. Novel D−π−A Structured Zn(Ii)-Porphyrin Dyes Containing a Bis(3,3-Dimethylfluorenyl)-Amine Moiety for Dye-Sensitised Solar Cells. *Chem. Commun.* **2012**, *48*, 9349.
(25) Jia, H.-L.; Li, S.-S.; Gong, B.-Q.; Gu, L.; Bao, Z.-L.; Guan, M.-Y. Efficient Cosensitization of New Organic Dyes Containing Bipyridine Anchors with Porphyrins for Dye-Sensitized Solar Cells. *Sustain. Energy Fuels* **2020**, *4*, 347−353.
(26) Sawhney, N.; Raghav, A.; Satapathi, S. Utilization of Naturally Occurring Dyes as Sensitizers in Dye Sensitized Solar Cells. *IEEE J. Photovoltaics* **2017**, *7*, 539−544.
(27) Kang, S. H.; Jeong, M. J.; Eom, Y. K.; Choi, I. T.; Kwon, S. M.; Yoo, Y.; Kim, J.; Kwon, J.; Park, J. H.; Kim, H. K. Porphyrin Sensitizers with Donor Structural Engineering for Superior Performance Dye-Sensitized Solar Cells and Tandem Solar Cells for Water Splitting Applications. *Adv. Energy Mater.* **2017**, *7*, 1602117.
(28) Luo, J.; Xu, M.; Li, R.; Huang, K.-W.; Jiang, C.; Qi, Q.; Zeng, W.; Zhang, J.; Chi, C.; Wang, P.; Wu, J. N -Annulated Perylene as An Efficient Electron Donor for Porphyrin-Based Dyes: Enhanced Light-Harvesting Ability and High-Efficiency Co(II/III)-Based Dye-Sensitized Solar Cells. *J. Am. Chem. Soc.* **2014**, *136*, 265−272.
(29) Yella, A.; Lee, H.-W.; Tsao, H. N.; Yi, C.; Chandiran, A. K.; Nazeeruddin, Md. K.; Diau, E. W.-G.; Yeh, C.-Y.; Zakeeruddin, S. M.; Grätzel, M. Porphyrin-Sensitized Solar Cells with Cobalt (II/III)−Based Redox Electrolyte Exceed 12 Percent Efficiency. *Science* **2011**, *334*, 629−634.
(30) Mishra, A.; Fischer, M. K. R.; Bäuerle, P. Metal-Free Organic Dyes for Dye-Sensitized Solar Cells: From Structure: Property Relationships to Design Rules. *Angew. Chem., Int. Ed.* **2009**, *48*, 2474−2499.
(31) Dulo, B.; Phan, K.; Githaiga, J.; Raes, K.; De Meester, S. Natural Quinone Dyes: A Review on Structure, Extraction Techniques, Analysis and Application Potential. *Waste Biomass Valorization* **2021**, *12*, 6339−6374.
(32) Qiu, H.-Y.; Wang, P.-F.; Lin, H.-Y.; Tang, C.-Y.; Zhu, H.-L.; Yang, Y.-H. Naphthoquinones: A Continuing Source for Discovery of Therapeutic Antineoplastic Agents. *Chem. Biol. Drug Des.* **2018**, *91*, 681−690.
(33) Chenab, K. K.; Sohrabi, B.; Zamani Meymian, M. R.; Mousav, S. V. Naphthoquinone Derivative-Based Dye for Dye-Sensitized Solar Cells: Experimental and Computational Aspects. *Mater. Res. Express* **2019**, *6*, 085537.
(34) Mahadik, S. A.; Pathan, H. M.; Salunke-Gawali, S.; Butcher, R. J. Aminonaphthoquinones as Photosensitizers for Mesoporous ZnO Based Dye-Sensitized Solar Cells. *J. Alloys Compd.* **2020**, *845*, 156279.
(35) Khanmohammadi, K.; Sohrabi, B.; Zamani Meymian, M. R. Effect of Electron-Donating and -Withdrawing Substitutions in Naphthoquinone Sensitizers: The Structure Engineering of Dyes for DSSCs. *J. Mol. Struct.* **2018**, *1167*, 274−279.
(36) Shinde, D.; Tambade, P.; Pathan, H.; Gadave, K. Experimental and Theoretical Study of 1, 4-Naphthoquinone Based Dye in Dye-Sensitized Solar Cells Using ZnO Photoanode. *Mater. Sci.* **2017**, *35*, 746−754.
(37) Khadtare, S. S.; Ware, A. P.; Salunke-Gawali, S.; Jadkar, S. R.; Pingale, S. S.; Pathan, H. M. Dye Sensitized Solar Cell with Lawsone Dye Using a ZnO Photoanode: Experimental and TD-DFT Study. *RSC Adv.* **2015**, *5*, 17647−17652.
(38) Sahoo, S. S.; Chadar, D.; Murmu, M.; Banerjee, P.; Salunke-Gawali, S.; Butcher, R. J. Evaluation of Physicochemical Properties of Provitamin K3 Derived Benzo[α]Phenoxazine as a Photosensitizer. *Eng. Sci.* **2021**, *14*, 94−108.
(39) Bhand, S.; Chadar, D.; Pawar, K.; Naushad, M.; Pathan, H.; Salunke-Gawali, S. Benzo[α]Phenothiazine Sensitized ZrO_2 Based Dye Sensitized Solar Cell. *J. Mater. Sci. Mater. Electron.* **2018**, *29*, 1034−1041.
(40) Mahadik, S. A.; Patil, A.; Pathan, H. M.; Butcher, R. J. Thionaphthoquinones as Photosensitizers for TiO_2 Nanorods ZnO Nanograin Based Dye-Sensitized Solar Cells: Effect of Nanostructures on Charge Transport and Photovoltaic Performance. *Eng. Sci.* **2020**, *14*, 46−58.
(41) Ardo, S.; Meyer, G. J. Photodriven heterogeneous charge transfer with transition-metal compounds anchored to TiO_2 semiconductor surfaces. *Chem. Soc. Rev.* **2009**, *38*, 115−164.
(42) Chen, Y.-S.; Li, C.; Zeng, Z. H.; Wang, W. B.; Wang, X. S.; Zhang, B. W. Efficient electron injection due to a special adsorbing group's combination of carboxyl and hydroxyl: dye-sensitized solar cells based on new hemicyanine dyes. *J. Mater. Chem.* **2005**, *15*, 1654−1661.
(43) Zhang, L.; Cole, J. M.; Waddell, P. G.; Low, K. S.; Liu, X. Relating electron donor and carboxylic acid anchoring substitution effects in azo dyes to dye-sensitized solar cell performance. *ACS Sustainable Chem. Eng.* **2013**, *1*, 1440−1452.
(44) Rajendra Prasad, M. B.; Kadam, V.; Joo, O.-S.; Pathan, H. M. Improving the Photovoltaic Parameters in Quantum Dot Sensitized Solar Cells through Employment of Chemically Deposited Compact Titania Blocking Layer. *Mater. Chem. Phys.* **2017**, *194*, 165−171.

https://doi.org/10.1021/acsomega.2c05334
ACS Omega 2022, 7, 41519−41530

(45) Rajendra Prasad, M. B.; Pathan, H. M. Room Temperature Synthesis of Rutile Titania Nanoparticles: A Thermodynamic Perspective. *Eur. Phys. J. D* **2014**, *68*, 25.
(46) Prasad M B, M. B. R.; Pathan, H. M. Effect of Photoanode Surface Coverage by a Sensitizer on the Photovoltaic Performance of Titania Based CdS Quantum Dot Sensitized Solar Cells. *Nanotechnology* **2016**, *27*, 145402.
(47) Vinaayak, S. B.; Balasubramani, V.; Shkir, M.; Manthrammel, M. A.; Sreedevi, G. Enhancing the performance of TiO_2 based N-DSSC using dye extracted from Cladophora Columbiana, Ludwigia repens and mixed sensitizer. *Opt. Mater.* **2022**, *133*, 112968.
(48) Liu, B.-Q.; Zhao, X.-P.; Luo, W. The synergistic effect of two photosynthetic pigments in dye-sensitized mesoporous TiO_2 solar cells. *Dyes Pigm.* **2008**, *76*, 327−331.
(49) Sahoo, S. S.; Salunke-Gawali, S.; Kadam, V. S.; Pathan, H. M. Canna Lily Red, and Yellow Flower Extracts, Yellow Flower Extracts: A New Power Source to Produce Photovoltage through Dye Sensitized Solar Cells. *Energy Fuels* **2020**, *34*, 9674−9682.
(50) Madhusudan Reddy, K.; Manorama, S. V.; Ramachandra Reddy, A. Bandgap Studies on Anatase Titanium Dioxide Nanoparticles. *Mater. Chem. Phys.* **2003**, *78*, 239−245.
(51) Waghmare, M. A.; Beedri, N. I.; Ubale, A. U.; Pathan, H. M. Fabrication and Characterization of Rose Bengal Sensitized Binary TiO2 -ZrO2 Oxides Photo-Electrode Based Dye-Sensitized Solar Cell. *Eng. Sci.* **2019**, *6*, 36−43.
(52) Welte, A.; Waldauf, C.; Brabec, C.; Wellmann, P. J. Application of Optical Absorbance for the Investigation of Electronic and Structural Properties of Sol-Gel Processed TiO2 Films. *Thin Solid Films* **2008**, *516*, 7256−7259.
(53) Sayyed, S. A. A. R.; Beedri, N. I.; Kadam, V. S.; Pathan, H. M. Rose Bengal Sensitized Bilayered Photoanode of Nano-Crystalline TiO2−CeO2 for Dye-Sensitized Solar Cell Application. *Appl. Nanosci.* **2016**, *6*, 875−881.
(54) Fujishima, A.; Rao, T. N.; Tryk, D. A. Titanium Dioxide Photocatalysis. *J. Photochem. Photobiol., C* **2000**, *1*, 1−21.
(55) Zhang, Q. Effects of Calcination on the Photocatalytic Properties of Nanosized TiO2 Powders Prepared by TiCl4 Hydrolysis. *Appl. Catal., B* **2000**, *26*, 207−215.
(56) Mani, J.; Sakeek, H.; Habouti, S.; Dietze, M.; Es-Souni, M. Macron−Meso-Porous TiO2, ZnO and ZnO−TiO_2 -Composite Thick Films. Properties and Application to Photocatalysiss. *Catal. Sci. Technol.* **2012**, *2*, 379−385.
(57) Inamdar, Y.; Beedri, N.; Kodam, K.; Shaikh, A.; Pathan, H. Aggregation of ZnO Nanocrystallites Using Polyol Process for Dye (Reactive Red) Sensitized Solar Cell: Aggregation of ZnO Nanocrystallites Using Polyol. *Macromol. Symp.* **2015**, *347*, 52−57.
(58) Sayyed, A. R.; Suhail, A.; Kadam, N. I.; Pathan, V. S.; Pathan, H. M. Rose Bengal-Sensitized Nanocrystalline Ceria Photoanode for Dye-Sensitized Solar Cell Application. *Bull. Mater. Sci.* **2016**, *39*, 1381−1387.
(59) Palomares, E.; Clifford, J. N.; Haque, S. A.; Lutz, T.; Durrant, J. R. Control of Charge Recombination Dynamics in Dye Sensitized Solar Cells by the Use of Conformally Deposited Metal Oxide Blocking Layers. *J. Am. Chem. Soc.* **2003**, *125*, 475−482.
(60) Kim, J. S.; Shin, S. S.; Han, H. S.; Shin, S.; Suk, J. H.; Kang, K.; Hong, K. S.; Cho, I. S. Facile Preparation of TiO_2 Nanobranch/Nanoparticle Hybrid Architecture with Enhanced Light-Harvesting Properties for Dye-Sensitized Solar Cells. *J. Nanomater.* **2015**, *2015*, 1−9.
(61) Jo, M.; Cho, J.; Wang, X.; Jin, E.; Jeong, S.; Kang, D.-W. Improving of the Photovoltaic Characteristics of Dye-Sensitized Solar Cells Using a Photoelectrode with Electrospun Porous TiO2 Nanofibers. *Nanomaterials* **2019**, *9*, 95.
(62) Moon, K. J.; Lee, S. W.; Lee, Y. H.; Kim, J. H.; Ahn, J. Y.; Lee, S. J.; Lee, D. W.; Kim, S. H. Effect of TiO2 Nanoparticle-Accumulated Bilayer Photoelectrode and Condenser Lens-Assisted Solar Concentrator on Light Harvesting in Dye-Sensitized Solar Cells. *Nanoscale Res. Lett.* **2013**, *8*, 283.
(63) Waghmare, M. A.; Beedri, N. I.; Baviskar, P. K.; Pathan, H. M.; Ubale, A. U. Effect of ZrO_2 Barrier Layers on the Photovoltaic Parameters of Rose Bengal Dye-Sensitized TiO2 Solar Cell. *J. Mater. Sci. Mater. Electron.* **2019**, *30*, 6015−6022.
(64) Ohno, T.; Sarukawa, K.; Tokieda, K.; Matsumura, M. Morphology of a TiO_2 Photocatalyst (Degussa, P-25) Consisting of Anatase and Rutile Crystalline Phases. *J. Catal.* **2001**, *203*, 82−86.
(65) Baiju, K. V.; Zachariah, A.; Shukla, S.; Biju, S.; Reddy, M. L. P.; Warrier, K. G. K. Correlating photoluminescence and photocatalytic activity of mixed-phase nanocrystalline titania. *Catal. Lett.* **2009**, *130*, 130−136.
(66) Meng, S.; Ren, J.; Kaxiras, E. Natural Dyes Adsorbed on TiO_2 Nanowire for Photovoltaic Applications: Enhanced Light Absorption and Ultrafast Electron Injection. *Nano Lett.* **2008**, *8*, 3266−3272.
(67) Maurya, I. C.; Neetu, A. K.; Gupta, P.; Srivastava, B. L.; Bahadur, L. Callindra haematocephata and Peltophorum pterocarpum flowers as natural sensitizers for TiO_2 thin film based dye-sensitized solar cells. *Opt. Mater.* **2016**, *60*, 270.
(68) Dandawate, F. V.; Kodolikar, J. G.; Kelkar, V. D.; Kulkarni, B. A. Thermal, Spectroscopic and Magnetic Studies of Some Rare Earth 3-Halolawsonemonoximates. *Thermochim. Acta* **1994**, *241*, 103−111.
(69) Jagtap, S. B.; Joshi, S. G.; Litake, G. M.; Ghole, V. S.; Kulkarni, B. A. C-3 Substituted Lawsonemonoximates of Holmium(III): Synthesis, Characterization, and Antimicrobial Activity. *Met.-Based Drugs* **2000**, *7*, 147−150.
(70) Pierpont, C. G.; Downs, H. H.; Rukavina, T. G. Neutral Tris(o-Benzoquinone) Complexes of Chromium, Molybdenum, and Tungsten. *J. Am. Chem. Soc.* **1974**, *96*, 5573−5574.
(71) Vandewal, K.; Benduhn, J.; Nikolis, V. C. How to Determine Optical Gaps and Voltage Losses in Organic Photovoltaic Materials. *Sustain. Energy Fuels* **2018**, *2*, 538−544.
(72) Cardona, C. M.; Li, W.; Kaifer, A. E.; Stockdale, D.; Bazan, G. C. Electrochemical Considerations for Determining Absolute Frontier Orbital Energy Levels of Conjugated Polymers for Solar Cell Applications. *Adv. Mater.* **2011**, *23*, 2367−2371.
(73) Yeoh, M.-E.; Chan, K.-Y. Recent Advances in Photo-Anode for Dye-Sensitized Solar Cells: A Review: Recent Advances in Photo-Anode for DSSCs: A Review. *Int. J. Energy Res.* **2017**, *41*, 2446−2467.
(74) Shaikh, J. S.; Shaikh, N. S.; Mali, S. S.; Patil, J. V.; Pawar, K. K.; Kanjanaboos, P.; Hong, C. K.; Kim, J. H.; Patil, P. S. Nanoarchitectures in Dye-Sensitized Solar Cells: Metal Oxides, Oxide Perovskites, and Carbon-Based Materials. *Nanoscale* **2018**, *10*, 4987−5034.
(75) Bramhankar, T. S.; Pawar, S. S.; Shaikh, J. S.; Gunge, V. C.; Beedri, N. I.; Baviskar, P. K.; Pathan, H. M.; Patil, P. S.; Kambale, R. C.; Pawar, R. S. Effect of Nickel−Zinc Co-Doped TiO2 Blocking Layer on Performance of DSSCs. *J. Alloys Compd.* **2020**, *817*, 152810.
(76) Raj, C. C.; Prasanth, R. A Critical Review of Recent Developments in Nanomaterials for Photoelectrodes in Dye Sensitized Solar Cells. *J. Power Sources* **2016**, *317*, 120−132.
(77) Yang, W.-G.; Wan, F.-R.; Chen, Q.-W.; Li, J.-J.; Xu, D.-S. Controlling Synthesis of Well-Crystallized Mesoporous TiO2 Microspheres with Ultrahigh Surface Area for High-Performance Dye-Sensitized Solar Cells. *J. Mater. Chem.* **2010**, *20*, 2870.
(78) Chen, J.; Wu, J.; Lei, W.; Song, J. L.; Deng, W. Q.; Sun, X. W. Co-Sensitized Quantum Dot Solar Cell Based on ZnO Nanowire. *Appl. Surf. Sci.* **2010**, *256*, 7438−7441.

https://doi.org/10.1021/acsomega.2c05334
ACS Omega 2022, 7, 41519−41530